

Supporting Information

Aqueous Biphasic Systems: A boost brought about by using ionic liquids

Mara G. Freire,^{*a} Ana Filipa M. Cláudio,^b João M. M. Araújo,^a João A. P. Coutinho,^b Isabel M. Marrucho,^{a,b} José N. Canongia Lopes,^c Luís Paulo N. Rebelo^{*a}

^aInstituto de Tecnologia Química e Biológica, ITQB2, Universidade Nova de Lisboa
(www.itqb.unl.pt), Av. República, Apartado 127, 2780-901 Oeiras, Portugal

^bDepartamento de Química, CICECO (www.ciceco.ua.pt), Universidade de Aveiro,
3810-193 Aveiro, Portugal

^cCentro de Química Estrutural, Instituto Superior Técnico (cqe.ist.utl.pt), 1049-001,
Lisboa, Portugal

*Corresponding author

Tel: +351 21 4469 441; Fax: +351 21 4411 277; E-mail address: maragfreire@ua.pt;
luis.rebelo@itqb.unl.pt.

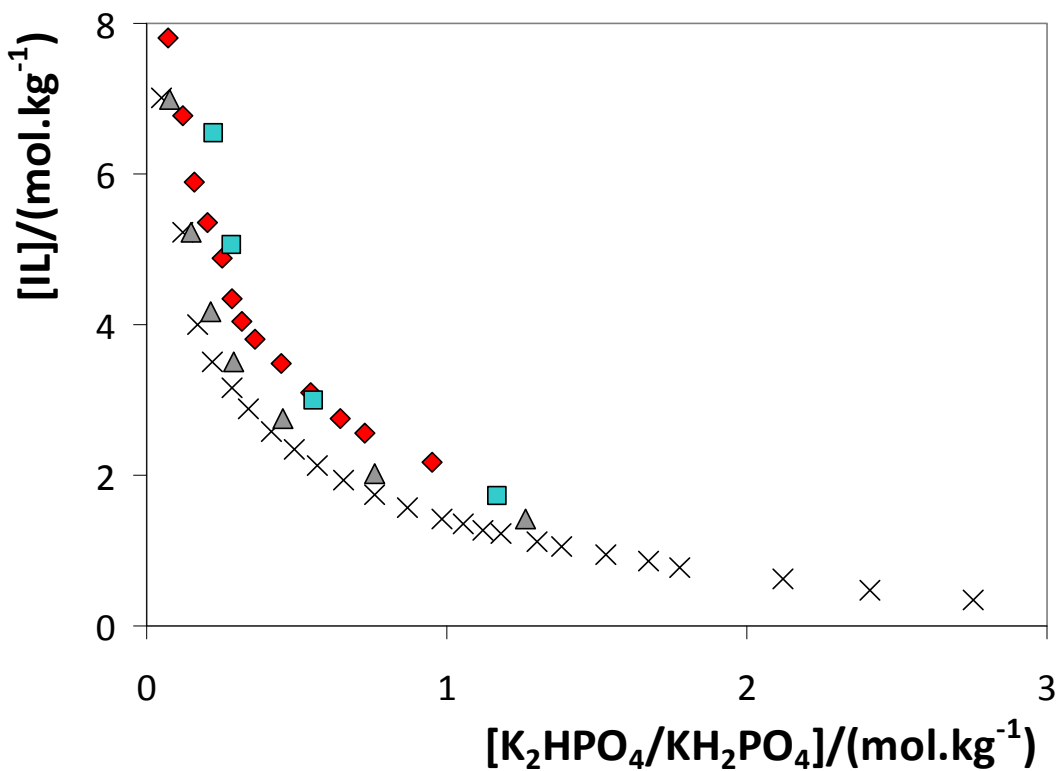


Fig. S1 Ternary phase diagrams for ABS composed of chloride-based ionic liquids + K₂HPO₄/KH₂PO₄ at 298 K: ■, [C₄C₁pyr]Cl; ◆, [C₄C₁im]Cl; ▲, [C₄C₁pip]Cl; ×, [C₄-3-C₁py]Cl.⁴⁵

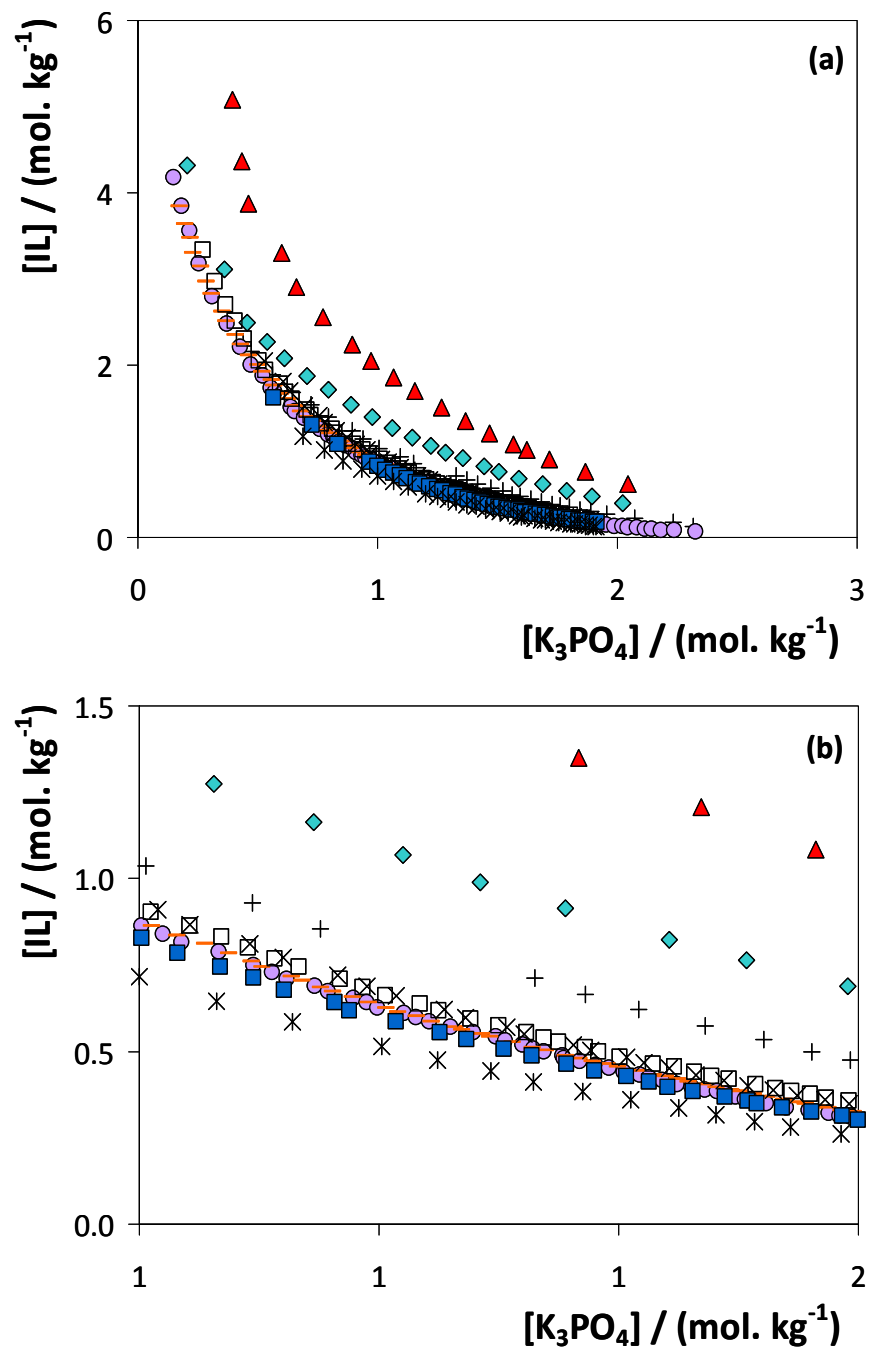


Fig. S2 Ternary phase diagrams for ABS composed of $[C_nC_1\text{im}]Cl$ ionic liquids + $K_3\text{PO}_4$ at 298 K: \blacktriangle , $[C_1C_1\text{im}]Cl$; \blacklozenge , $[C_2C_1\text{im}]Cl$; $+$, $[C_4C_1\text{im}]Cl$; \bullet , $[C_6C_1\text{im}]Cl$; $-$, $[C_7C_1\text{im}]Cl$; \square , $[C_8C_1\text{im}]Cl$; \times , $[C_{10}C_1\text{im}]Cl$; \blacksquare , $[C_{12}C_1\text{im}]Cl$; $*$, $[C_{14}C_1\text{im}]Cl$.¹⁸ (b) is an expansion of (a).

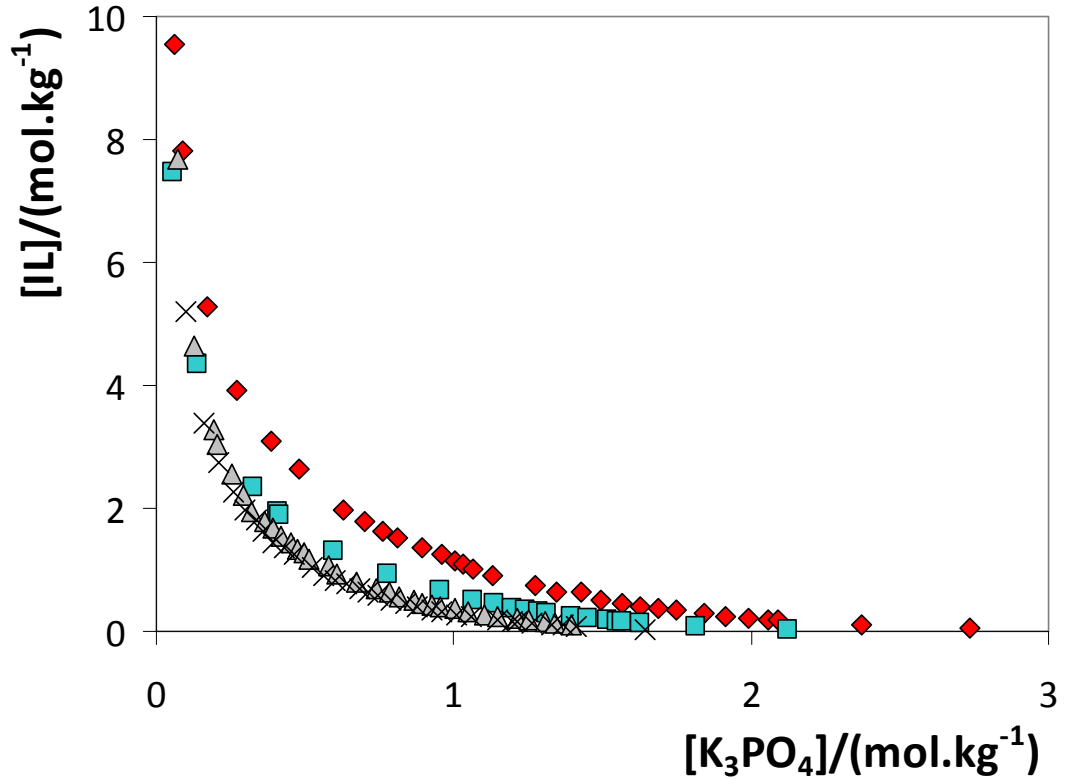


Fig. S3 Ternary phase diagrams for ABS composed of $[C_2C_1\text{im}]$ -based ionic liquids + K_3PO_4 at 298.15 K: ♦, $[C_2C_1\text{im}][C_1\text{SO}_4]$; ■, $[C_2C_1\text{im}][C_4\text{SO}_4]$; ▲, $[C_2C_1\text{im}][C_6\text{SO}_4]$; ×, $[C_2C_1\text{im}][C_8\text{SO}_4]$.¹¹

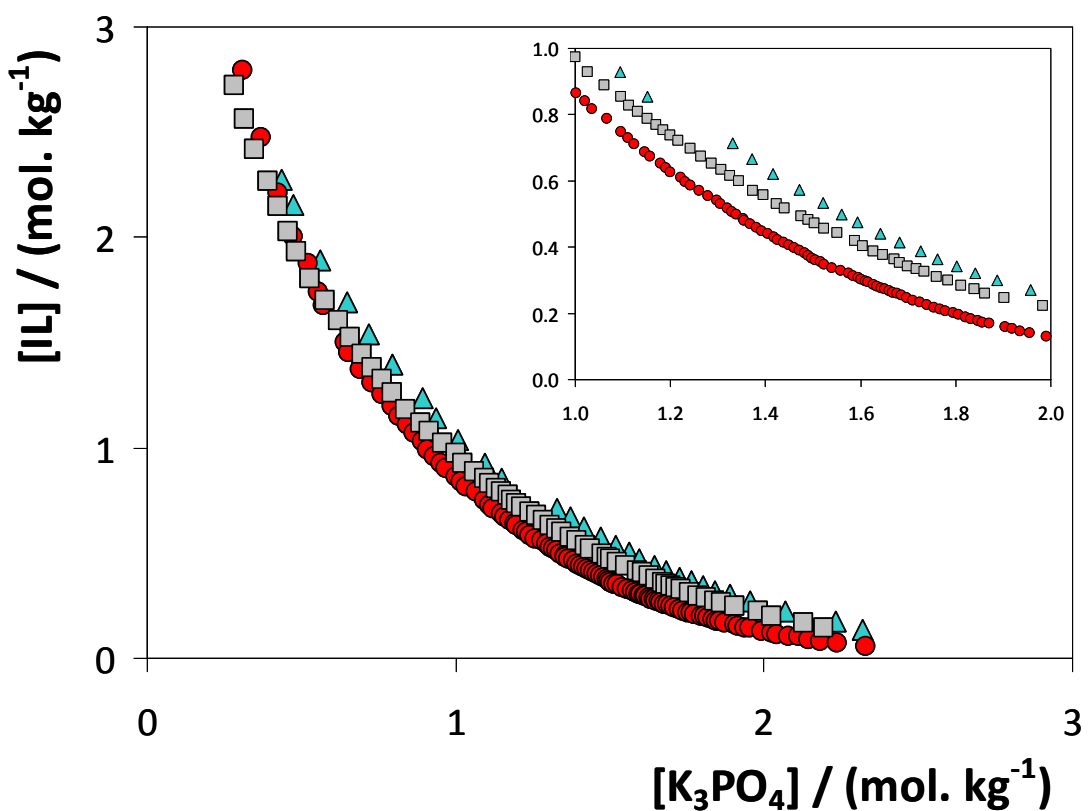


Fig. S4 Ternary phase diagrams for ABS composed of imidazolium-based ionic liquids + K_3PO_4 at 298 K: ■, $[C_4C_1C_1\text{im}]Cl$; ▲, $[C_4C_1\text{im}]Cl$; ●, $[C_6C_1\text{im}]Cl$.¹⁸

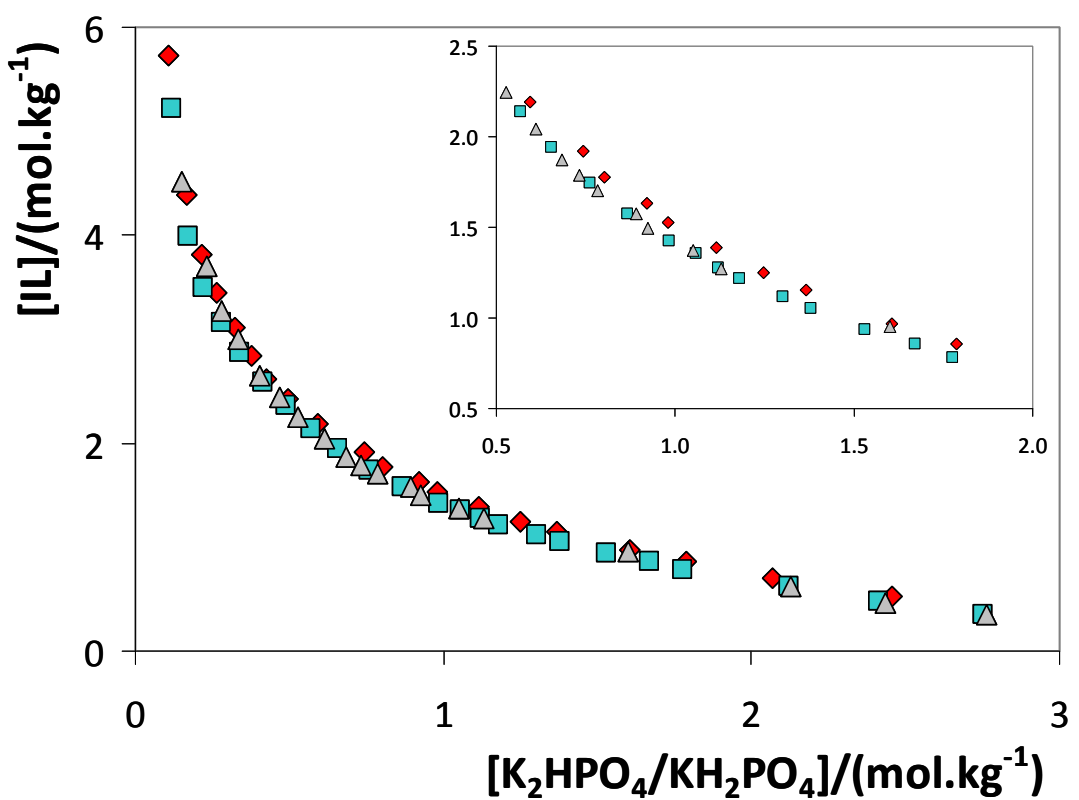


Fig. S5 Ternary phase diagrams for ABS composed of pyridinium-chloride-based ionic liquids + $\text{K}_2\text{HPO}_4/\text{KH}_2\text{PO}_4$ at 298 K: \blacklozenge , $[\text{C}_4\text{-2-C}_1\text{py}] \text{Cl}$; \blacksquare , $[\text{C}_4\text{-3-C}_1\text{py}] \text{Cl}$; \blacktriangle , $[\text{C}_4\text{-4-C}_1\text{py}] \text{Cl}$.⁴⁵

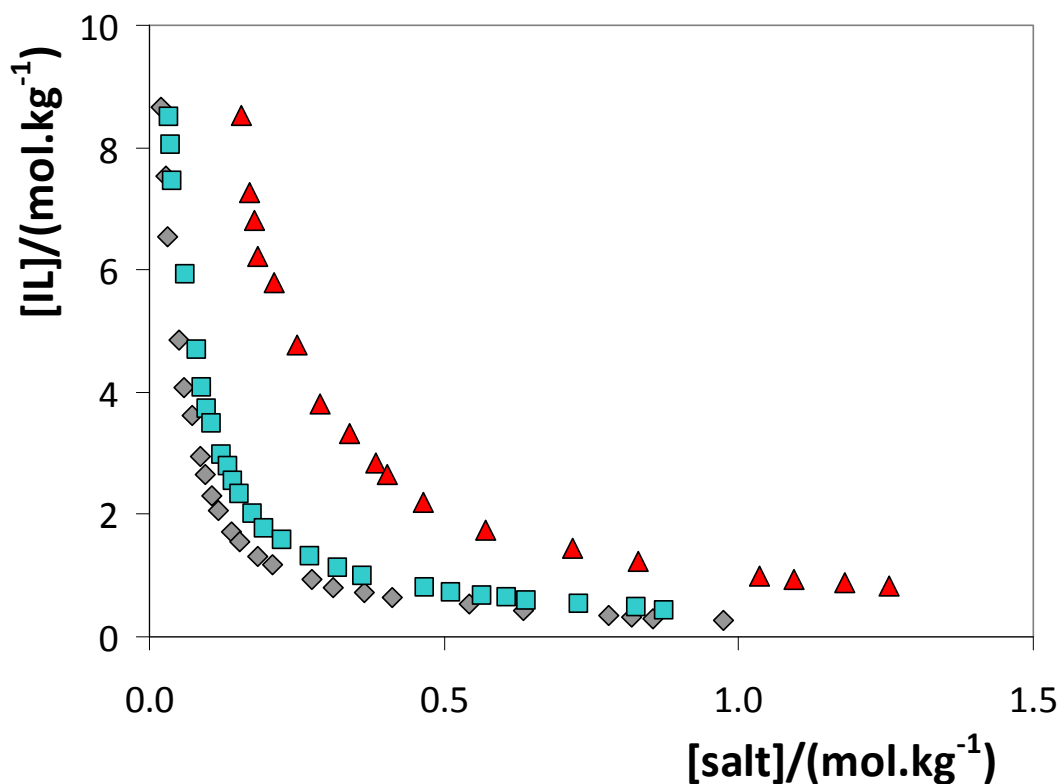


Fig. S6 Ternary phase diagrams for ABS composed of [C₄C₁im][BF₄] + sodium-based salts at 298.15 K: ▲, NaCH₃CO₂; ■, Na₂C₄H₄O₆; ◆, Na₃C₆H₅O₇.²¹

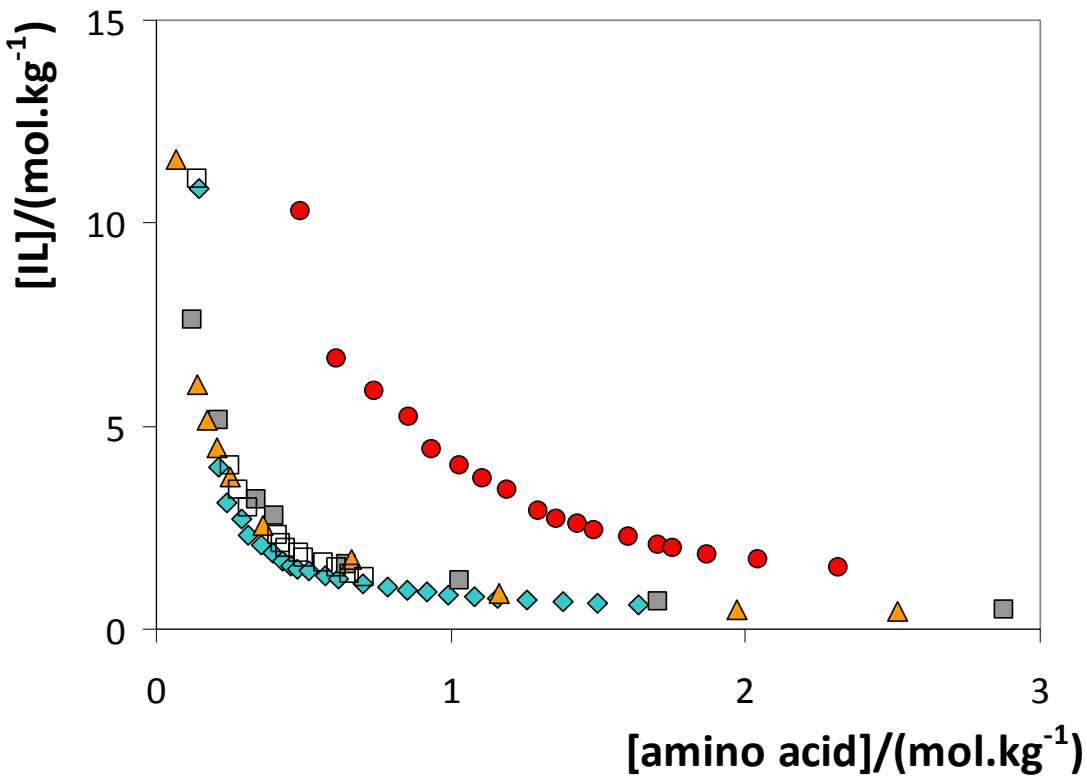


Fig. S7 Ternary phase diagrams for ABS composed of $[C_4C_1\text{im}][BF_4]$ + amino acids at 298 K: ●, L-proline; ■, glycine; ▲, L-serine; □, D,L-lysine·HCl; ♦, L-lysine.^{14,58}

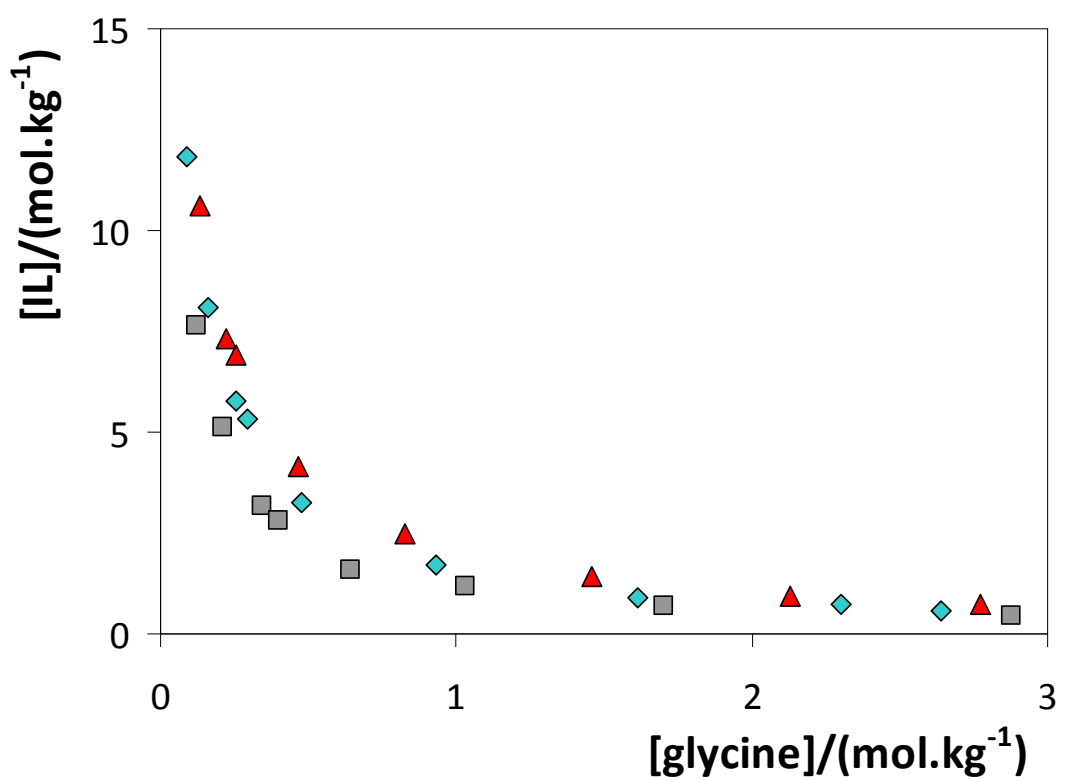


Fig. S8 Ternary phase diagrams for ABS composed of $[\text{C}_4\text{C}_1\text{im}][\text{BF}_4]$ + lysine at: ■, 298 K; ♦, 308.15 K; ▲, 318.15 K.⁵⁸

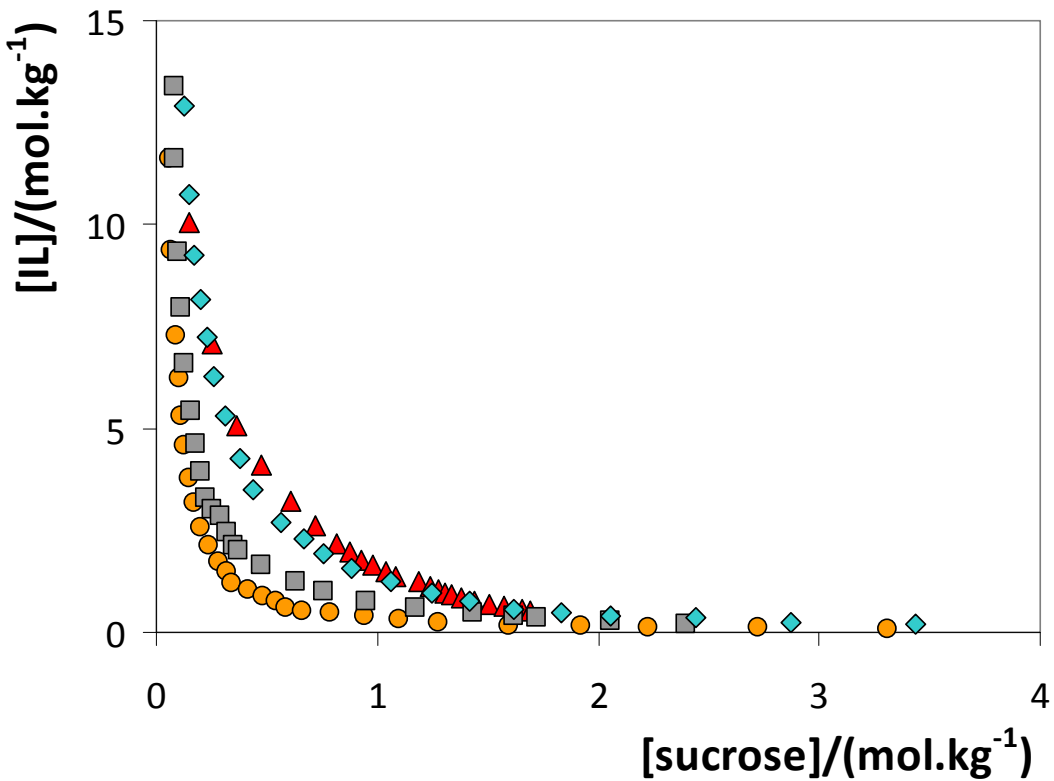


Fig. S9 Ternary phase diagrams for ABS composed of ionic liquids + sucrose at 298 K:
▲, $[\text{C}_4\text{C}_1\text{im}][\text{CF}_3\text{SO}_3]$; ♦, $[\text{aC}_1\text{im}]\text{Cl}$; ■, $[\text{aC}_1\text{im}]\text{Br}$; ●, $[\text{C}_4\text{C}_1\text{im}][\text{BF}_4]$.^{17,51}

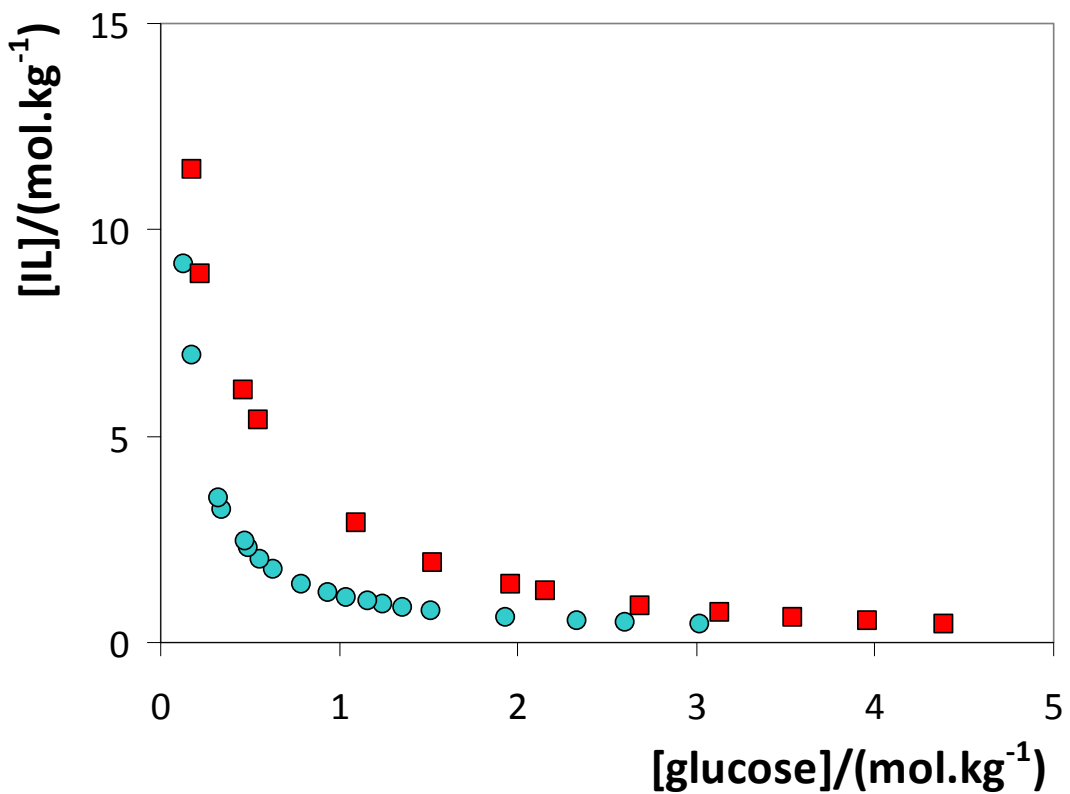


Fig. S10 Ternary phase diagrams for ABS composed of ionic liquids + glucose at 298 K:

■, [C₃C₁im][BF₄]; ●, [C₄C₁im][BF₄].⁸

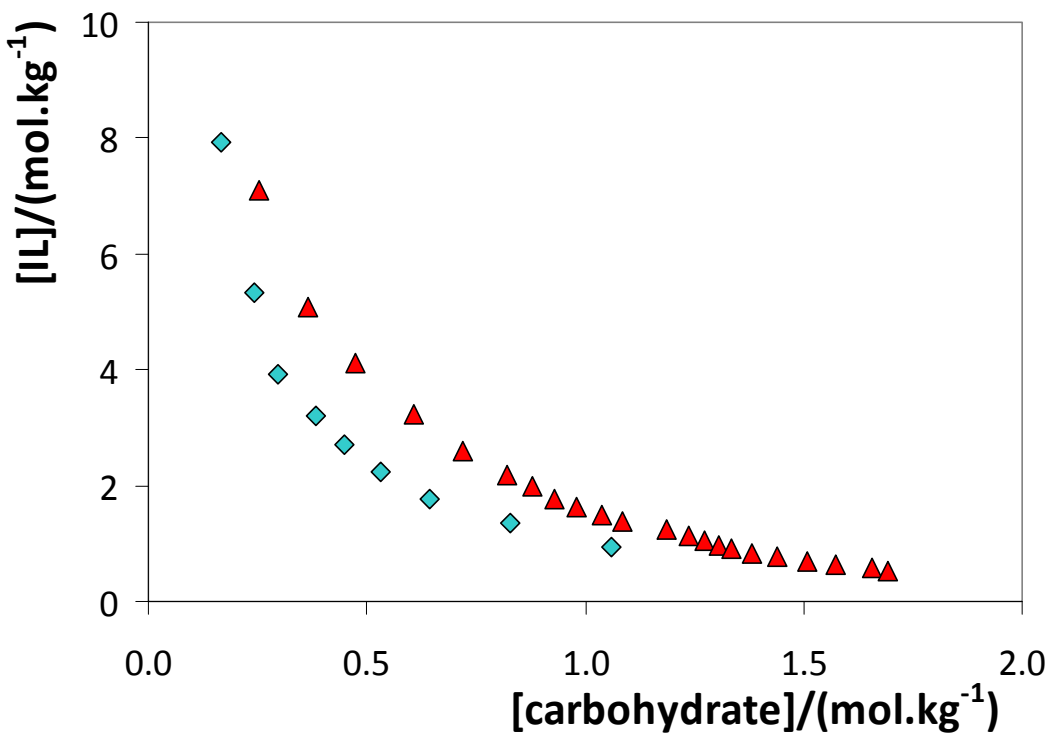


Fig. S11 Ternary phase diagrams for ABS composed of $[\text{C}_4\text{C}_1\text{im}][\text{CF}_3\text{SO}_3]$ + dissacharides at 298 K: \blacklozenge , D-(+)-maltose; \blacktriangle , sucrose.¹⁷

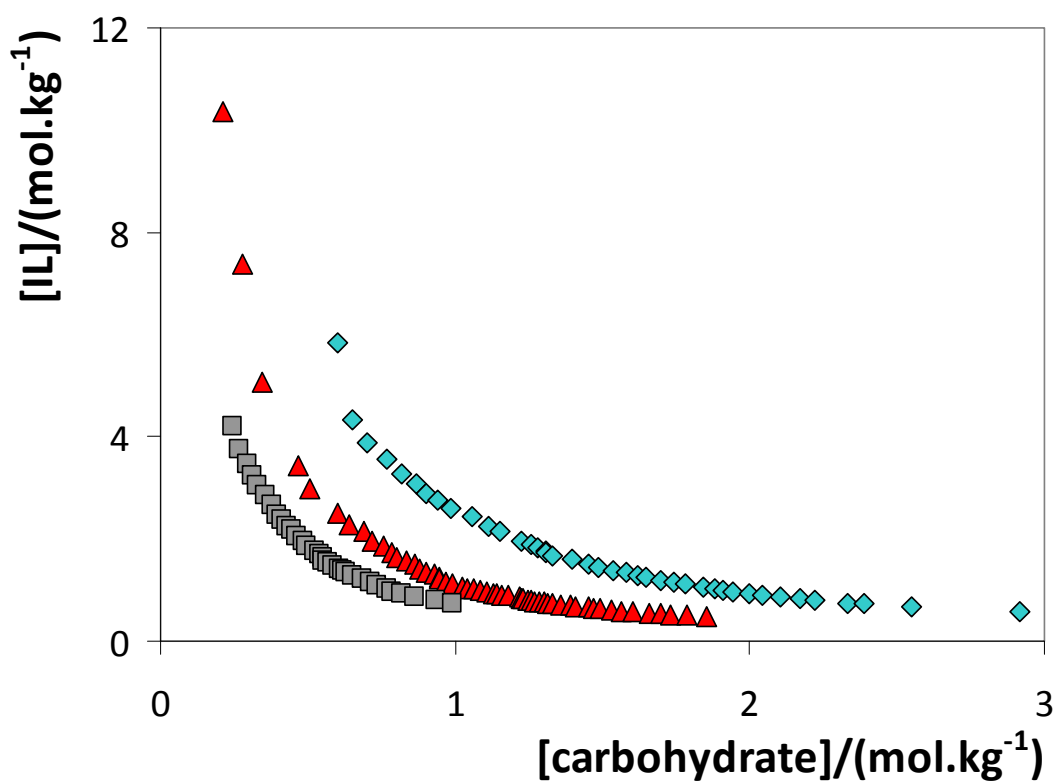


Fig. S12 Ternary phase diagrams for ABS composed of [C₄C₁im][CF₃SO₃] + polyols at 298 K: ■, D-maltitol; ▲, D-sorbitol; ◆, xylitol.¹⁷

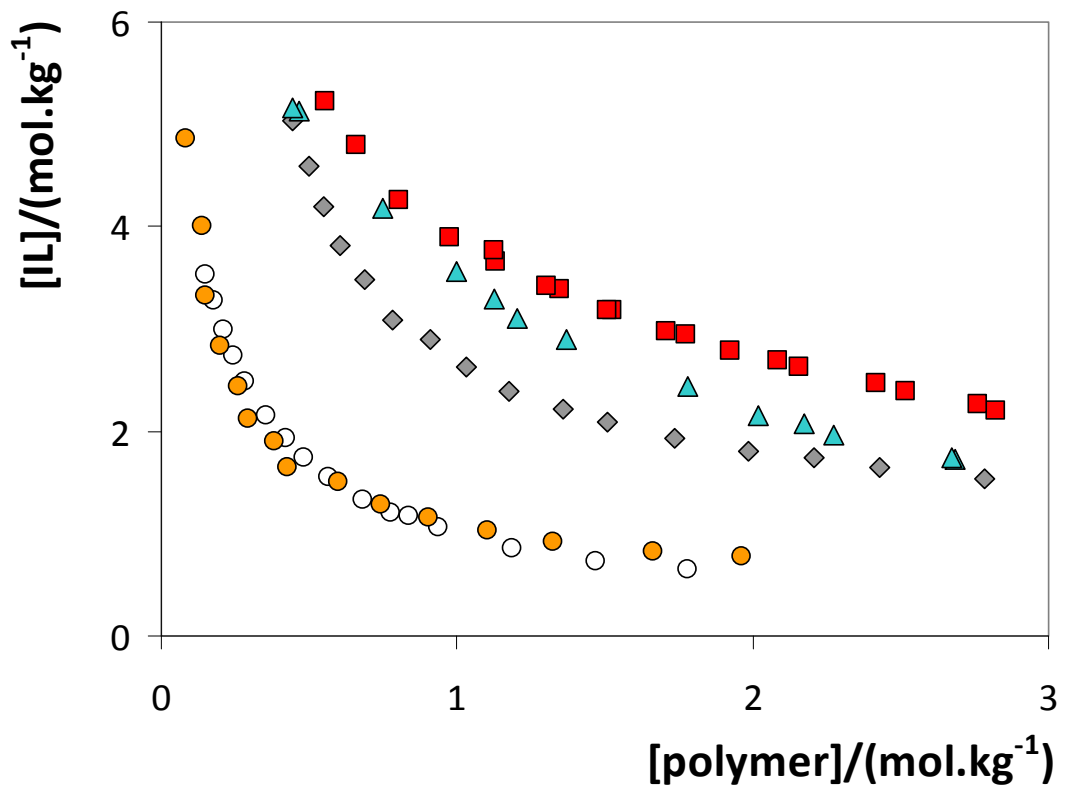


Fig. S13 Ternary phase diagrams for ABS composed of ionic liquid + PPG 400 at 298 K:
■, $[\text{C}_4\text{C}_1\text{im}]\text{Br}$; ▲, $[\text{C}_2\text{C}_1\text{im}]\text{Br}$; ◆, $[\text{C}_4\text{C}_1\text{im}]\text{Cl}$; ○, $[\text{aC}_1\text{im}]\text{Cl}$; ●, $[\text{C}_4\text{C}_1\text{im}][\text{C}_1\text{CO}_2]$.⁶³⁻⁶⁴

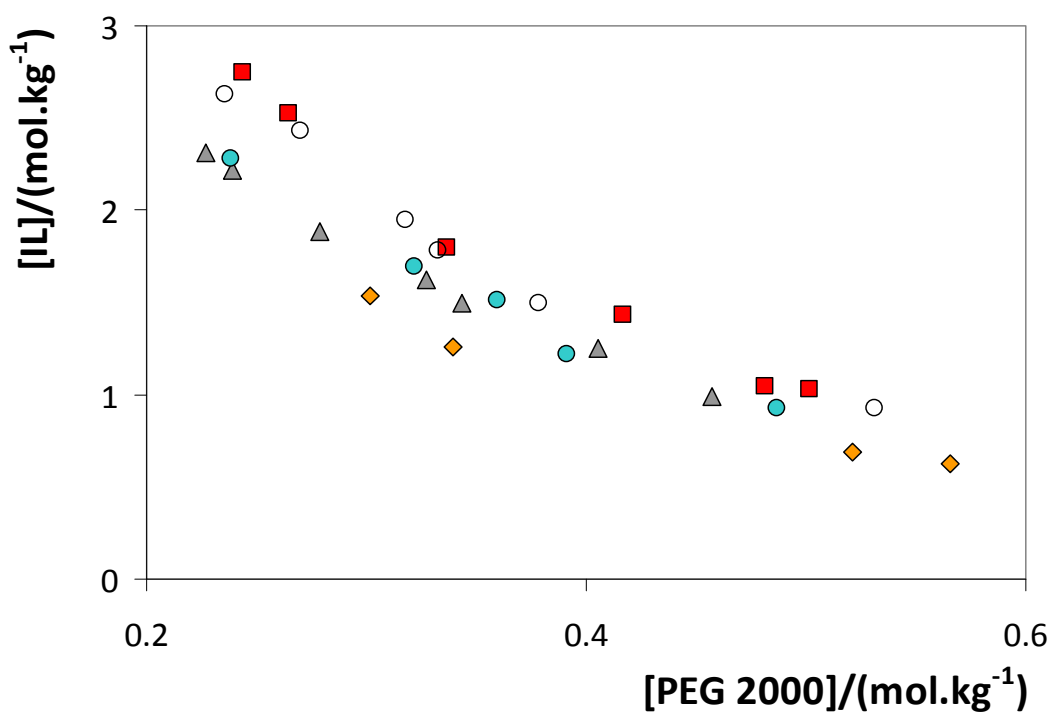


Fig. S14 Ternary phase diagrams for ABS composed of ionic liquid + PEG 2000 at 298 K: ■, [C₄C₁im]Cl; ○, [C₄C₁py]Cl; ●, [C₄C₁pyr]Cl; ▲, [C₄C₁pip]Cl; ♦, [P₄₄₄₄]Cl.⁶⁰

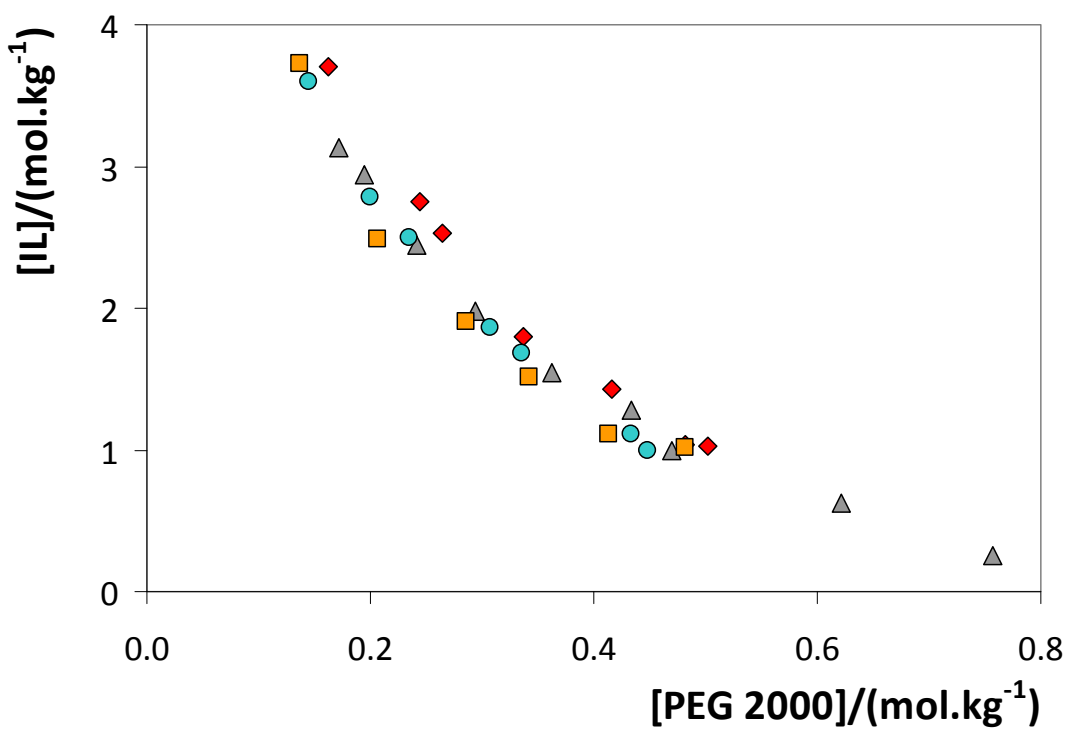


Fig. S15 Ternary phase diagrams for ABS composed of ionic liquid + PEG 2000 at 298 K:
K: \blacklozenge , $[\text{C}_4\text{C}_1\text{im}] \text{Cl}$; \blacktriangle , $[\text{C}_2\text{C}_1\text{im}] \text{Cl}$; \bullet , $[\text{aC}_1\text{im}] \text{Cl}$; \blacksquare , $[\text{OHC}_2\text{C}_1\text{im}] \text{Cl}$.⁶⁰

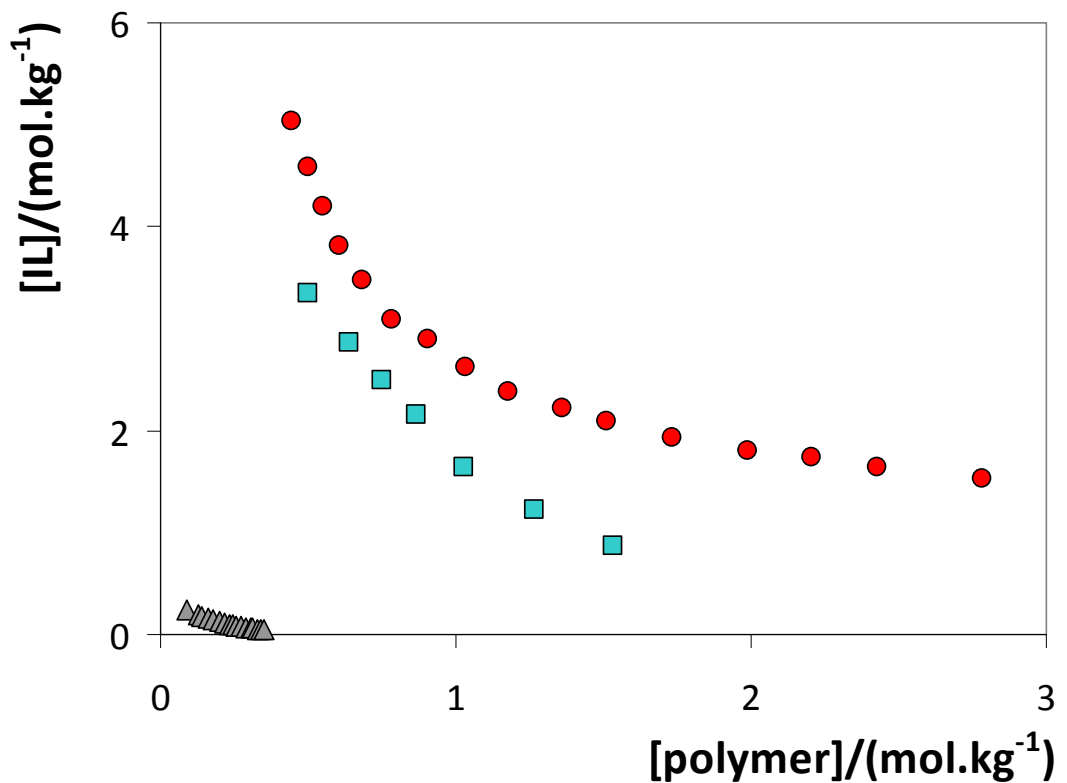


Fig. S16 Ternary phase diagrams for ABS composed of [C₄C₁im]Cl + polymer at 298 K:
●, PPG 400; ■, PEG 1000; ▲, PPG 1000.^{60,63}

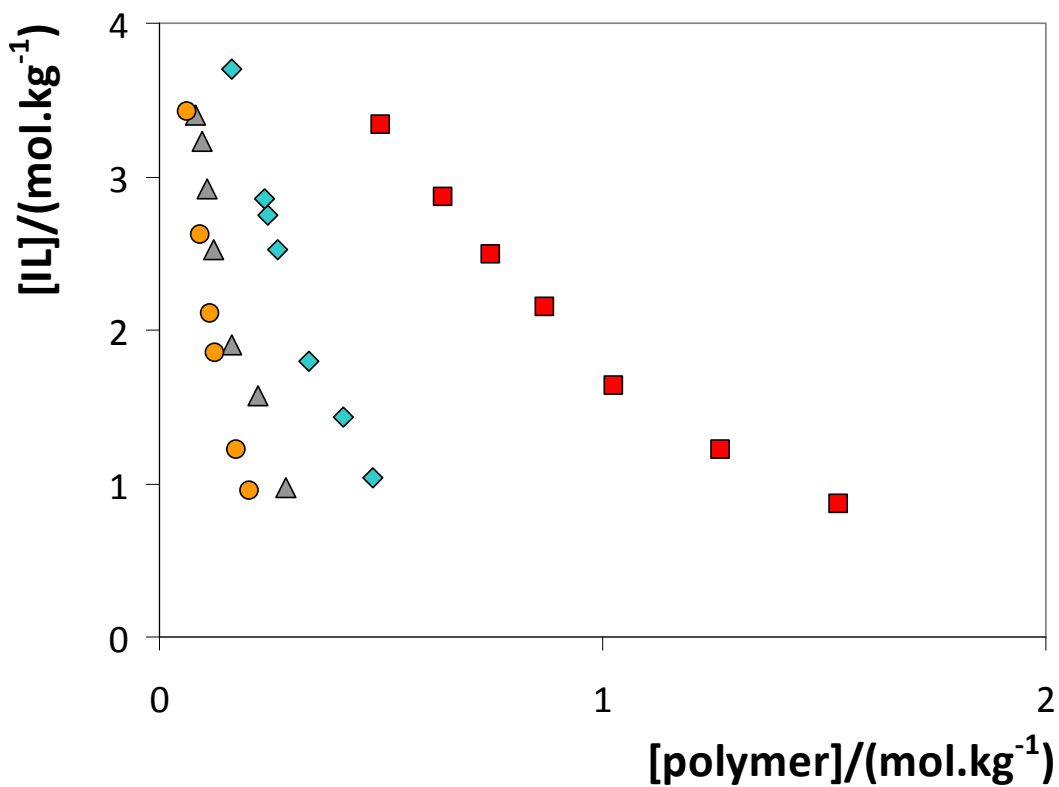


Fig. S17 Ternary phase diagrams for ABS composed of $[\text{C}_4\text{C}_1\text{im}] \text{Cl} + \text{polymer}$ at 298 K:
■, PEG 1000; ◆, PEG 2000; ▲, PEG 3400; ●, PEG 4000.⁶⁰

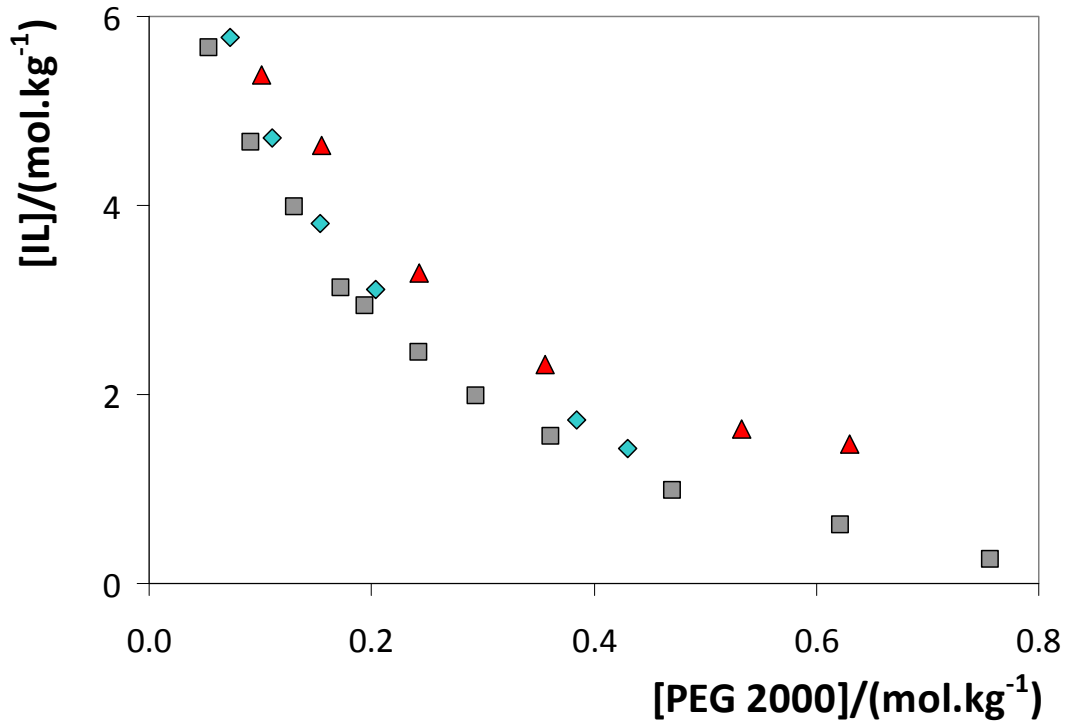


Fig. S18 Ternary phase diagrams for ABS composed of $[C_2C_1im]Cl + PEG\ 2000$ at: \blacktriangle , 323 K; \blacklozenge , 308 K; \blacksquare , 298 K.⁶⁰

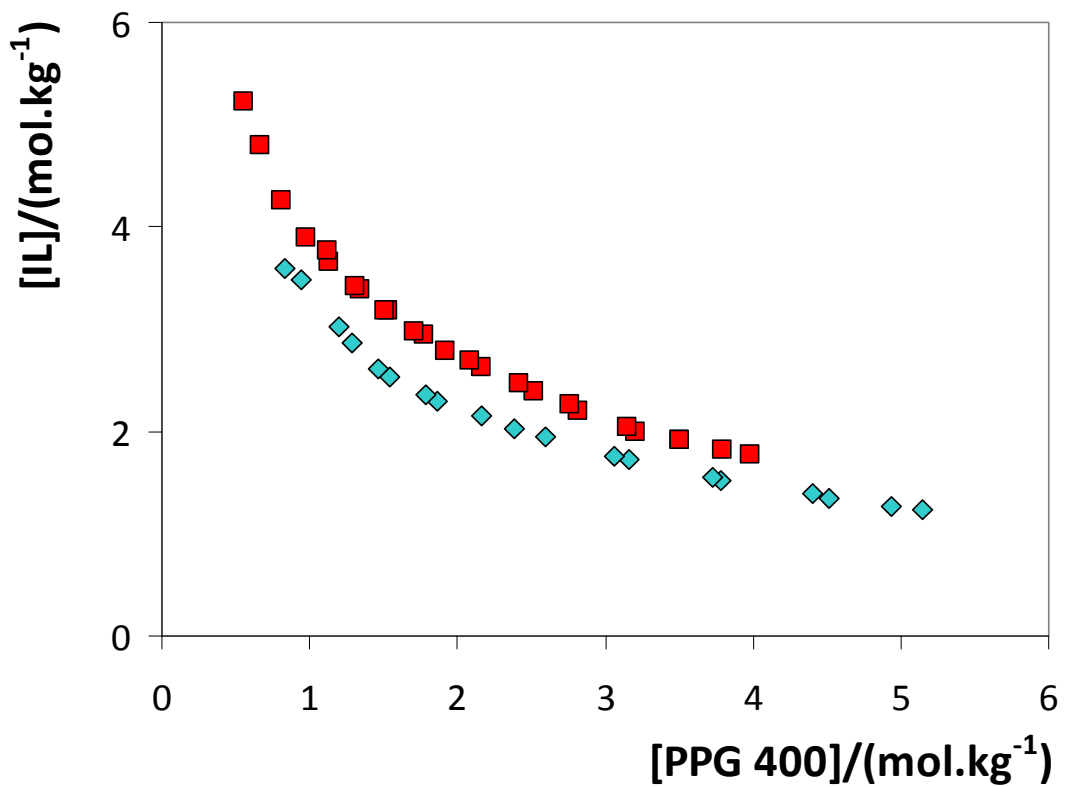


Fig. S19 Ternary phase diagrams for ABS composed of $[\text{C}_2\text{C}_1\text{im}]\text{Br}$ + PPG 400 at: ■, 298.15 K; ◆, 318.15 K.⁶⁴

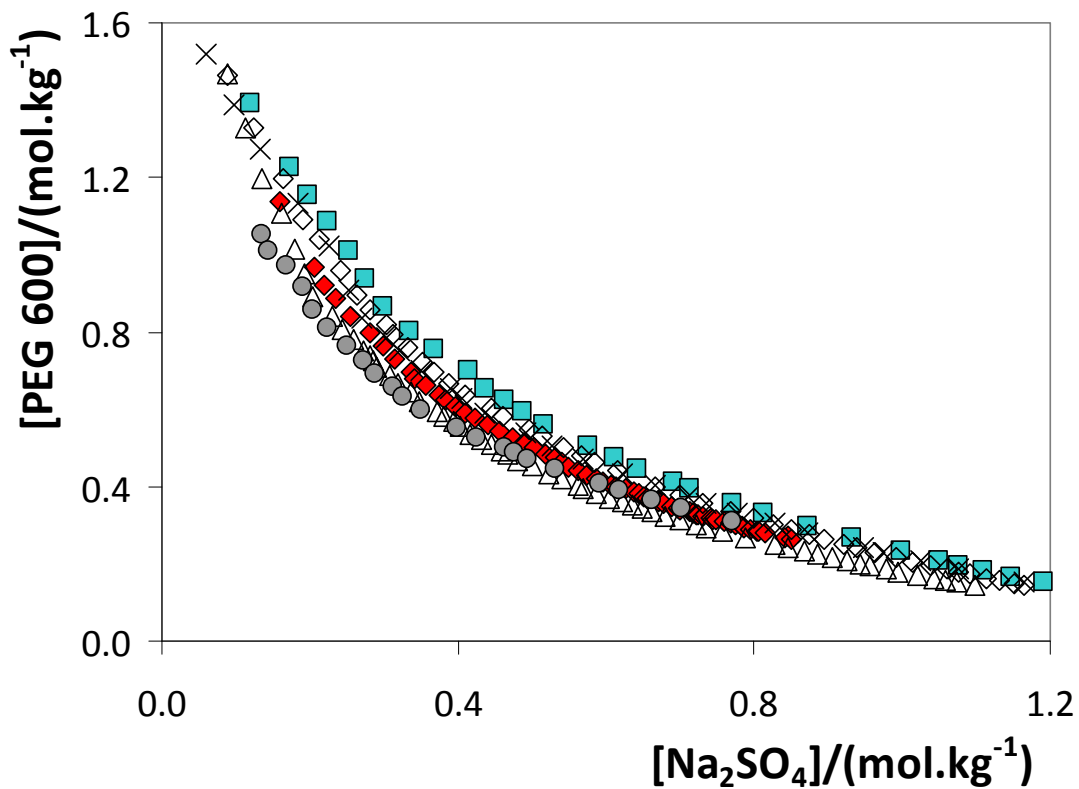


Fig. S20 Phase diagrams for ABS composed of PEG 600 + Na_2SO_4 + 5 wt % ionic liquid at 298 K: \blacklozenge , no ionic liquid; ■, $[\text{im}]Cl$; \lozenge , $[\text{C}_1\text{im}]Cl$; \times , $[\text{C}_2\text{C}_1\text{im}]Cl$; Δ , $[\text{C}_4\text{C}_1\text{im}]Cl$; ●, $[\text{C}_4\text{C}_1\text{C}_1\text{im}]Cl$.⁶¹

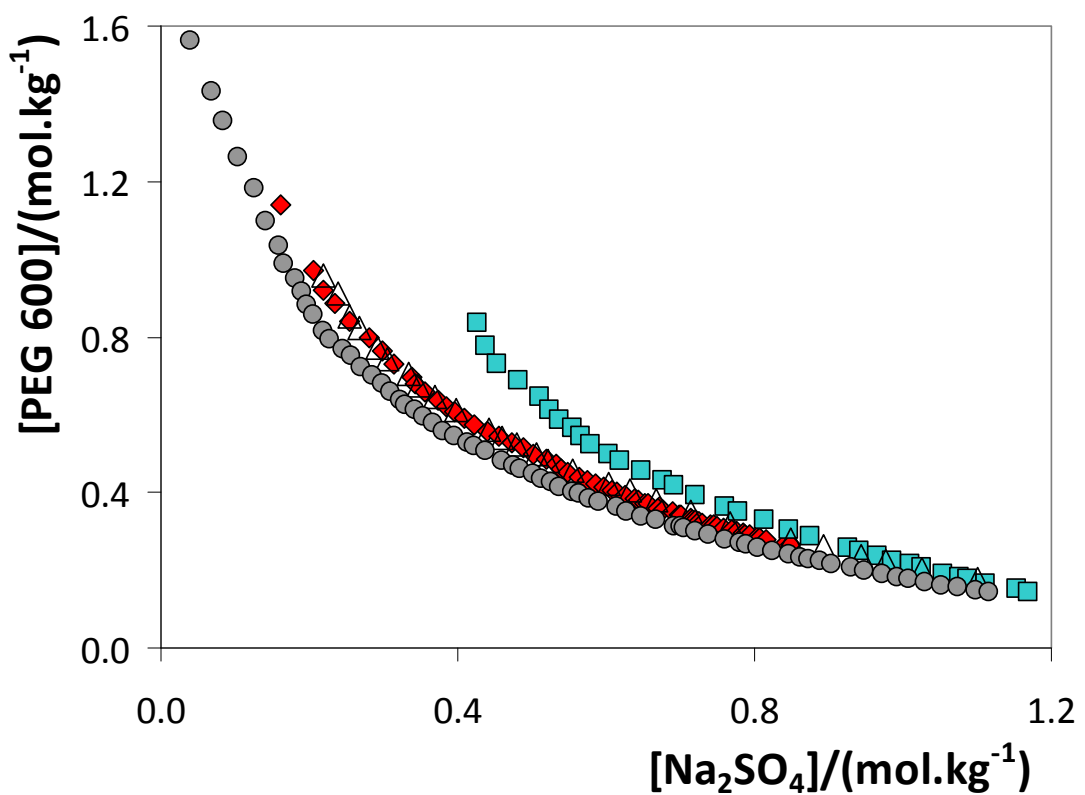


Fig. S21 Phase diagrams for ABS composed of PEG 600 + Na₂SO₄ + 5 wt % ionic liquid at 298 K: ♦, no ionic liquid; ■, [OHC₂C₁im]Cl; △, [aC₁im]Cl, ●, [C₇H₇C₁im]Cl.⁶¹

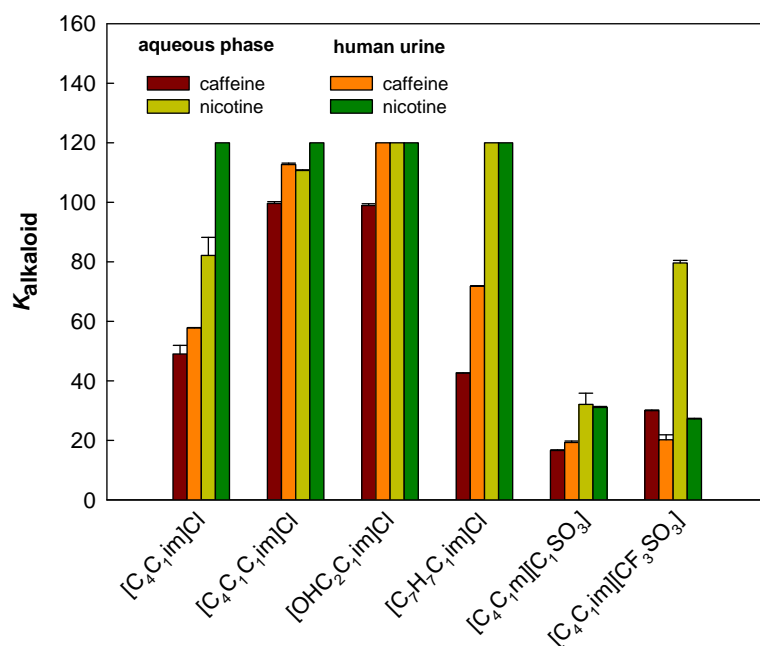


Fig. S22 Partition coefficients of caffeine and nicotine in different ABS at 298 K, obtained from the direct extraction of alkaloids from a synthetic biological sample – artificial human urine – and from simple aqueous phases.⁷⁴

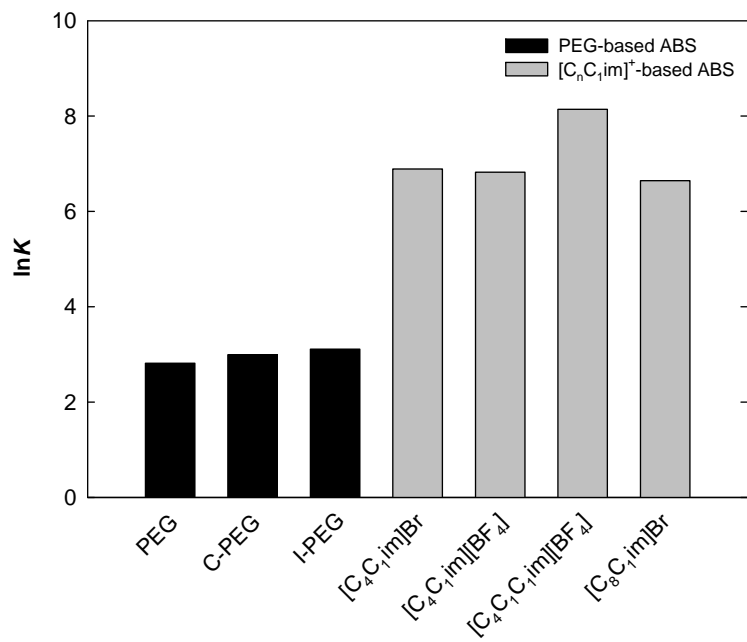


Fig. S23 Comparison of the partition coefficients of penicillin in ABS composed of several imidazolium-based ionic liquids and NaH_2PO_4 or Na_2HPO_4 .^{26,90}

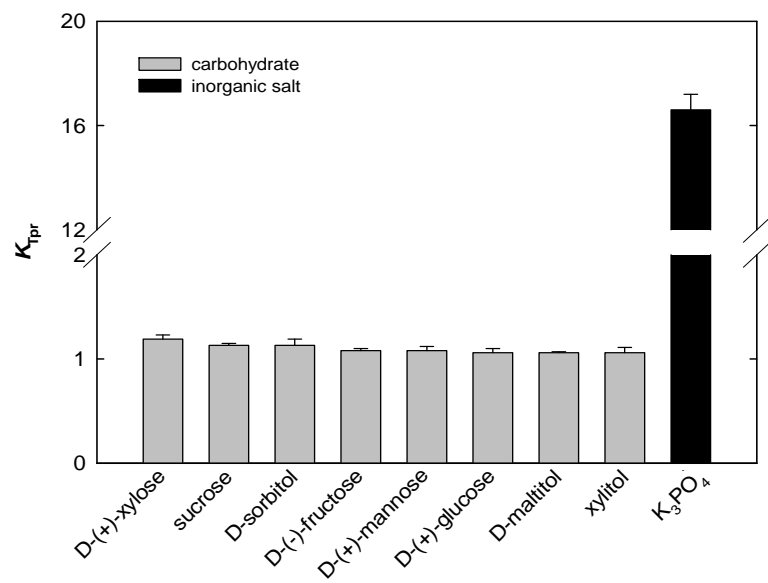


Fig. S24 Partitioning coefficients of L-tryptophan between $[C_4C_1\text{im}][CF_3\text{SO}_3]$ - and carbohydrate-rich aqueous phases at 298 K. The effect of inorganic salt $K_3\text{PO}_4$ on the partition coefficient is also depicted to address the extraction efficiency of carbohydrates.^{17,43}

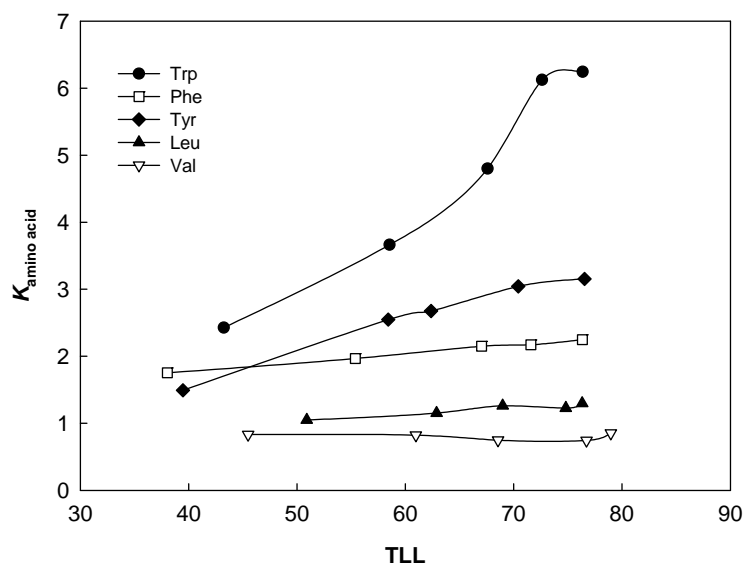


Fig. S25 Effect of the tie-line length (TLL) on the partitioning coefficients of amino acids for the $[\text{C}_4\text{C}_1\text{im}]\text{Br}$ + potassium citrate/citric acid + H_2O ABS at pH = 6, a pH close to the isoelectric point, at 298.15 K.⁹⁵

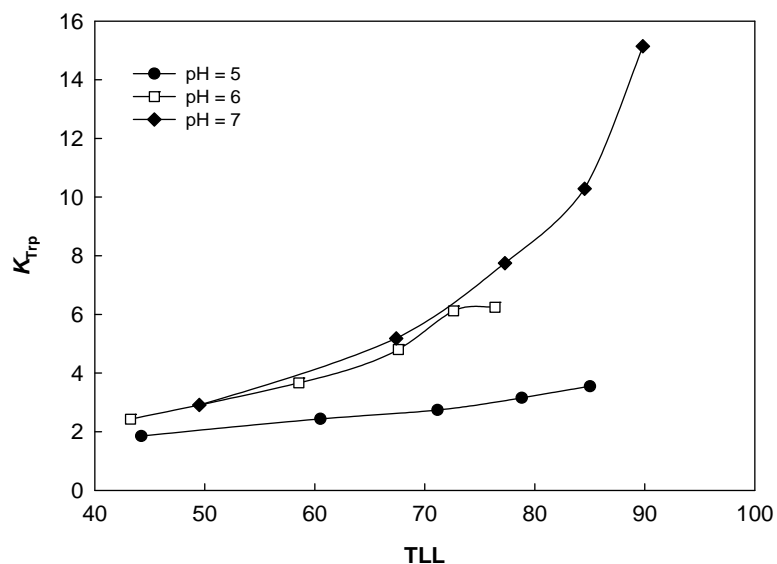


Fig. S26 Effect of the pH on the partitioning coefficients of tryptophan in the $[\text{C}_4\text{C}_1\text{im}]\text{Br}$ + potassium citrate/citric acid + H_2O ABS at 298.15 K.⁹⁵